

large degrees of interaction (>50% crystallization of olivine). Model parameters: $U_{\text{wedge}} = 3$ ppb, $U_{\text{melt}} = 0.2$ ppm, $r = 0.1$, $D_{\text{wedge}} = 6 \times 10^{-3}$.

19. In fertile peridotite, clinopyroxene remains a residual phase until ~22% melting [A. L. Jaques and D. H. Green, *Contrib. Mineral. Petrol.* **73**, 287 (1980)]. However, peridotites depleted by ~7% melt extraction, such as the Tinaquillo spinel ilherzolite, contain less clinopyroxene;

consequently, this ceases to be a residual phase after only ~8% partial melting [J. A. C. Robinson and B. J. Wood, *Earth Planet. Sci. Lett.* **164**, 277 (1998); L. E. Wasylenski, M. B. Baker, M. M. Hirschmann, E. M. Stolper, *Eos (Fall Suppl.)* **77**, F847 (1996)].

20. We are grateful to A. Ewart, T. Worthington, S. Acland, J. Pearce, A. Reay, I. Smith, and J. Gamble for their generosity in providing samples and to J. L.

Joron for his help. We also thank C. Hawkesworth for helpful discussions and careful reading of the manuscript. Careful reviews by R. Arculus and anonymous reviewers led to significant improvements. B.B. was funded by CNRS and S.T. by a Royal Society Research Fellowship. This is IGP contribution no. 1647.

24 August 1999; accepted 2 November 1999

Gas-Rich Galaxy Pair Unveiled in the Lensed Quasar 0957+561

P. Planesas,^{1*} J. Martín-Pintado,¹ R. Neri,² L. Colina³

Molecular gas in the host galaxy of the lensed quasar 0957+561 (QSO 0957+561) at the redshift of 1.41 has been detected in the carbon monoxide (CO) line. This detection shows the extended nature of the molecular gas distribution in the host galaxy and the pronounced lensing effects due to the differentially magnified CO luminosity at different velocities. The estimated mass of molecular gas is about 4×10^9 solar masses, a molecular gas mass typical of a spiral galaxy like the Milky Way. A second, weaker component of CO is interpreted as arising from a close companion galaxy that is rich in molecular gas and has remained undetected so far. Its estimated molecular gas mass is 1.4×10^9 solar masses, and its velocity relative to the main galaxy is 660 kilometers per second. The ability to probe the molecular gas distribution and kinematics of galaxies associated with high-redshift lensed quasars can be used to improve the determination of the Hubble constant H_0 .

Little is known about the contents of molecular gas in galaxies or quasi-stellar objects (quasars) at high redshift, and even less is known about the molecular gas distribution and kinematics. Such knowledge is essential to understanding the evolution of galaxies that are experiencing phases of high activity, in the form of active galactic nuclei or a massive starburst. The relation of the quasar phenomenon to galaxy interaction or merger (1) and to star formation activity (2) and its possible evolutionary link with luminous infrared galaxies (3) are the subjects of a debate that could be better framed if molecular gas distribution and kinematics at high redshift were available. Indeed, the molecular gas presumably constitutes the reservoir that feeds the quasar and the star formation activity (4).

Gravitational lenses have recently become a powerful tool for probing the molecular gas content in galaxies at high redshift ($z > 1$). At present, CO emission, the best tracer of molecular gas mass, has been detected in nine objects at redshifts between 2.3 and 4.7 (5). Magnification of the emitted spectral lines by a gravitational lens has helped to make the CO emission detectable in at least five cases

(5). All of these objects, except the quasar APM 08279+5255 (6), appear to be one order of magnitude richer in molecular gas than the Milky Way, making them prime candidates for huge starbursts that could not be maintained for a long period of time. It has been suggested that the exhaustion of the molecular gas could lead to the end of the quasar activity (7) and eventually to the evolution of the host galaxy, an interacting spiral, toward an elliptical galaxy (8).

Between 6 May and 25 December of 1998, we observed the 3.1-mm radio continuum and the CO $2 \rightarrow 1$ (9) emission of the twin QSO 0957+561, the first example of gravitational lensing, unambiguously identified 20 years ago (10). We used the radio interferometer of the Institut de Radio Astronomie Millimétrique (IRAM) located at Plateau de Bure (France). Three interferometer configurations of the five 15-m-diameter antennas were used, giving 27 hours of useful data on the source and an angular resolution of $3.2''$ by $3.1''$. The radio continuum (Fig. 1) and the spectral line of CO (Fig. 2) were detected. The line appears redshifted to 95.5 GHz for $z = 1.4141$. Simultaneous observation at the redshifted frequency of the CO $5 \rightarrow 4$ line (238.7 GHz) gave no detection of such a line or of the radio continuum because of insufficient sensitivity at this higher observing frequency. The 3σ limit for the line detection was 5.5 mJy per beam [1 jansky (Jy) = 10^{-26} W m⁻² Hz⁻¹] for a velocity resolution of 50 km s⁻¹.

The radio continuum map at a wavelength

of 3.1 mm (Fig. 1) shows three components that, within the measurement uncertainties, agree in position with optical images A and B (11), whereas source C is the northeastern lobe of the radio jet associated with A (12). The integrated fluxes for sources A, B, and C are 4.4, 2.6, and 7.2 mJy, respectively. The B/A flux ratio is 0.6, similar to the ratio obtained at lower frequencies with the Very Large Array (VLA) radio interferometer (13) and in the near infrared (14). The 20-mm to 3-mm spectral index for quasar images A and B is $\alpha = -0.6$ ($S \propto \nu^\alpha$), which is somewhat less steep than that at longer wavelengths (S is the flux at a frequency ν).

The picture that emerges from the CO $2 \rightarrow 1$ line observations (Table 1 and Fig. 2) is much more complex than that of the radio continuum and optical images (11). Two images, CO-A and CO-B, lay close to the radio and optical A and B images (Table 1), separated from them by $\sim 0.4''$. The CO-B image is a highly distorted arc, extended in the east-west direction. A third image of the molecular gas emission, CO-F, with no counterpart in the radio continuum or optical wavelengths, is connected to the CO-B image by a weak arclike structure. The resulting overall picture is interpreted as being produced by the lens acting on an extended distribution of the molecular gas in the host galaxy. Arcs are

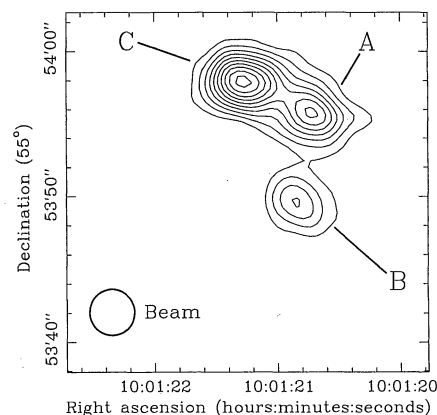


Fig. 1. Radio continuum contour map of the lensed quasar 0957+561, at a wavelength of 3.1 mm. Source C is the radio continuum jet associated with image A of the quasar. The lensing galaxy is located $\sim 1''$ north of image B (11). Contour levels are in steps of 0.5 mJy per beam, ranging from 0.5 to 5.0 mJy per beam. The absolute position of sources A and B coincides with that of the VLA (13) measurements, within measurement uncertainties. The synthesized beam of $3.2''$ by $3.1''$ is shown in the lower left corner.

¹Observatorio Astronómico Nacional (IGN), Apartado 1143, E-28800 Alcalá de Henares, Spain. ²Institut de Radio Astronomie Millimétrique, F-38460 Saint Martin d'Hères, France. ³Instituto de Física de Cantabria (CSIC-UC), Facultad de Ciencias, E-39005 Santander, Spain.

*To whom correspondence should be addressed. E-mail: planesas@oan.es

known to be produced when the source covers a fraction of a caustic line of the lens (15). Caustics separate regions of different image multiplicity; therefore, CO-F could be produced by the fraction of the molecular gas that extends over the inner caustic located $\sim 1''$ (5.7 kpc) south of the quasar, according to a recent model for this gravitational lens (16). Assuming a symmetric distribution for the molecular gas centered in the quasar, we found a lower limit of $2''$ (12 kpc) for the angular size of the gas distribution in the quasar host galaxy.

A further confirmation of the effects of the lens acting on the extended distribution of molecular gas comes from an inspection of the line profiles obtained toward the CO sources (Table 1 and Fig. 2). Emission in CO-B extends over the velocity range from -450 to $+150$ km s^{-1} , with the line peak velocity of -190 km s^{-1} (equivalent to a redshift of $z = 1.4116$), as determined by a Gaussian fit. The line emission from the CO-F source is one-third as strong as the CO-B line and is less extended in the velocity range. Moreover, the peak velocity is redshifted by ~ 60 km s^{-1} with respect to the peak velocity for the profile toward CO-B. This velocity difference may indicate that molecular

gas is distributed in a rotating disk in which the southernmost part, the one located south of the inner caustic, is moving toward Earth. This is an important aspect of these observations because galactic rotation in an extended disk can produce different profiles in the images of the lensed galaxy and can thus provide a means of studying the galactic kinematics.

The line profile taken toward the CO-A image shows two velocity components. The blue component peaks at about the same velocity as CO-B. The red component peaks at a velocity that is 660 km s^{-1} higher than the blue one, equivalent to a redshift of $z = 1.4238$. This component appears only toward the CO-A source. If the red and blue components arise from the quasar host galaxy, the kinematics of the molecular gas cannot be explained. The bluest part of the CO emission would have to be located south of the inner caustic to explain the CO-F profile and north of the outer caustic to explain the CO-A profile. Moreover, the line width for the total CO-A line profile is ~ 1000 km s^{-1} , wider by almost a factor of 2 than the widest CO profile found in quasars and ultraluminous infrared galaxies, that of Arp 220 (17). An alternative is that the red component comes

from a second object, a molecular gas-rich galaxy, that has not been detected in previous observations. The companion galaxy to the quasar host galaxy would be located a few tenths of an arc second toward the north of the quasar ($0.3'' = 1.7$ kpc), above the outer northern caustic of the lens, as the radio jets producing the C component are (Fig. 1). Like the radio continuum jets, only one image of the companion galaxy is produced, and it is located close to the image A of the quasar. The strong quasar emission has prevented the companion galaxy's detection at optical wavelengths, and its radio continuum emission is probably too weak to be detected.

The total molecular gas mass of the two galaxies can be estimated from the intrinsic CO luminosity L'_{CO} , measured in the CO profiles and corrected for the magnification by the gravitational lens. The magnification factor is probably different for each profile and can only be evaluated through detailed modeling if the two-dimensional distribution of the molecular gas emission is known. We assumed it to be the same as the optical magnification factor, $m \sim 10$, for every component. We used the usual value for the CO luminosity to H_2 mass conversion factor of $M(\text{H}_2)/L'_{\text{CO}} = 4 M_{\odot} (\text{K km s}^{-1} \text{pc}^2)^{-1}$ (18) to estimate the mass, where M_{\odot} is the solar mass. The molecular gas masses estimated from the emission toward the quasar host galaxy observed in images A and B are 2×10^9 and $6 \times 10^9 M_{\odot}$, respectively, for a luminosity distance of 6.9 Gpc (here we adopted Hubble constant $H_0 = 75 \text{ km s}^{-1} \text{ Mpc}^{-1}$ and deceleration parameter $q_0 = 0.5$). This mass is similar to the molecular gas mass of the Milky Way and is distributed in a disk that is several kiloparsecs in diameter. The molecular gas mass of the companion galaxy is $1.4 \times 10^9 M_{\odot}$. These masses are one order of magnitude smaller than the masses found in the host galaxies of quasars at $2 < z < 5$, typically between 10^{10} and $10^{11} M_{\odot}$ (5). The preferential detection of quasar host galaxies with such a large molecular gas mass may arise from observational selection effects, favoring the detection of the most luminous objects. Even in these extreme objects, the molecular gas will be transformed into stars in $< 10^8$ years, the typical lifetime of a quasar (19).

Our observations show that radio spectroscopy of molecular lines with high-angular and high-velocity resolution of lensed objects at cosmological distances is able to reveal the effects of the lens on different parts of the lensed galaxy, even if it is spatially unresolved by the highest angular resolution currently available. The extended distribution of molecular gas can be traced by the different images produced at different velocity ranges. These multiple images will help to better constrain the lens model, the main source of uncertainty in the determination of H_0 , from the delay time of optical and radio continuum intensity variations.

Fig. 2. Contour map of the integrated intensity of the CO $2 \rightarrow 1$ emission. The contour levels are 0.45, 0.65, 0.85, and 1.05 Jy km s^{-1} . The three CO images are elongated and show some structure, as expected from the extended nature of the molecular gas in the host galaxy of the quasar. In the radio continuum map (Fig. 1), sources A and B appear pointlike, as expected from emission coming from the quasar. Line profiles corresponding to images CO-A, CO-B, and CO-F are shown next to the contour map. The velocity resolution is 57 km s^{-1} , and the origin of the velocity scale corresponds to the redshift $z = 1.4141$. The contribution of the radio continuum has been subtracted from the line map and the line profiles.

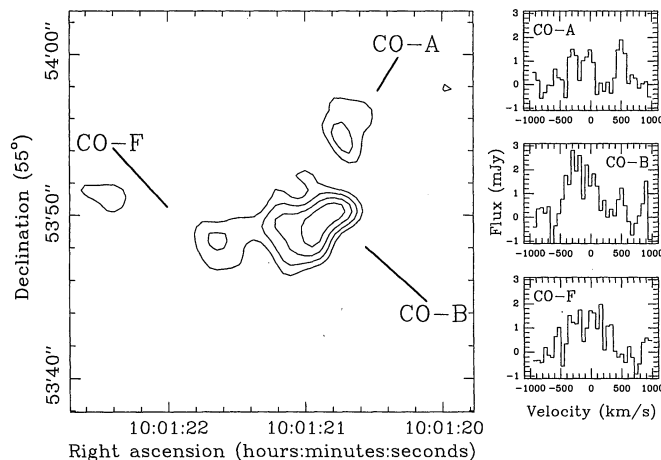


Table 1. Observed and derived properties of the CO $2 \rightarrow 1$ emission. CO-A-red refers to the CO emission associated with the red component, presumably arising from a gas-rich companion galaxy to the quasar host galaxy. The line parameters were determined by a Gaussian fit. RA, right ascension; Dec, declination; rc, radio continuum.

Component	CO-A	CO-A-red	CO-B	CO-F
$RA_{\text{CO}} - RA_{\text{rc}}$	$-0.3''$	NA	$+0.5''$	NA
$Dec_{\text{CO}} - Dec_{\text{rc}}$	$-0.1''$	NA	$-0.2''$	NA
Peak line flux (mJy)	1.1	1.7	2.3	1.4
Line width (km s^{-1})	380	160	500	250
Peak velocity* (km s^{-1})	-160	500	-190	-130
Integrated line flux (Jy km s^{-1})	0.45	0.30	1.22	0.38
Molecular gas mass† (M_{\odot})	2.2×10^9	1.4×10^9	6.1×10^9	1.8×10^9

*Velocities refer to $V = 0$ for $z = 1.4141$. †A magnification factor of 10 was used to obtain the gas mass; we adopted $H_0 = 75 \text{ km s}^{-1} \text{ Mpc}^{-1}$ and $q_0 = 0.5$.

References and Notes

- J. N. Bahcall, S. Kirhakos, D. H. Saxe, D. P. Schneider, *Astrophys. J.* **479**, 642 (1997).
- J. B. Hutchings, D. Crampton, S. L. Morris, D. Durand, E. Steinbring, *Astron. J.* **117**, 1109 (1999).
- D. B. Sanders, B. T. Soifer, J. H. Elias, G. Neugebauer, K. Matthews, *Astrophys. J. Lett.* **328**, L35 (1988).
- N. Z. Scoville, S. Padin, D. B. Sanders, B. T. Soifer, M. S. Yun, *Astrophys. J. Lett.* **415**, L75 (1993).
- F. Combes, R. Maoli, A. Omont, *Astron. Astrophys.* **345**, 369 (1999).
- D. Downes, R. Neri, T. Wiklind, D. J. Wilner, P. A. Shaver, *Astrophys. J. Lett.* **513**, L1 (1999).
- D. B. Sanders *et al.*, *Astrophys. J.* **325**, 74 (1988).
- J. Kormendy and D. B. Sanders, *Astrophys. J. Lett.* **390**, L53 (1992).
- CO 2 \rightarrow 1 is the transition from the rotational quantum level $J = 2$ to $J = 1$ of the carbon monoxide molecule. The observed frequency is given by $\nu_0/(1+z)$, where ν_0 is the rest (laboratory) frequency and z is the redshift.
- D. Walsh, R. F. Carswell, R. J. Weymann, *Nature* **279**, 381 (1979).
- A. Stockton, *Astrophys. J. Lett.* **242**, L141 (1980).
- P. E. Greenfield, D. H. Roberts, B. F. Burke, *Science* **208**, 495 (1980).
- M. Harvanek, J. T. Stocke, J. A. Morse, G. Rhee, *Astron. J.* **114**, 2240 (1997).
- B. T. Soifer *et al.*, *Nature* **285**, 91 (1980).
- J. N. Hewitt, E. L. Turner, D. P. Schneider, B. F. Burke, G. I. Langston, *Nature* **333**, 537 (1988).
- R. Barkana *et al.*, *Astrophys. J.* **520**, 479 (1999).
- K. Sakamoto *et al.*, *Astrophys. J.* **514**, 68 (1999).
- S. J. E. Radford, D. Downes, P. M. Solomon, *Astrophys. J. Lett.* **368**, L15 (1991).
- M. G. Haehnelt and M. J. Rees, *Mon. Not. R. Astron. Soc.* **263**, 168 (1993).
- We thank the IRAM staff at Plateau de Bure for their assistance. Supported by the Spanish Dirección General de Enseñanza superior under project PB96-104.

23 August 1999; accepted 29 October 1999

Enhanced Morphine Analgesia in Mice Lacking β -Arrestin 2

Laura M. Bohn,^{1*} Robert J. Lefkowitz,^{2,†} Raul R. Gainetdinov,¹ Karsten Peppel,² Marc G. Caron,^{1,†} Fang-Tsy Lin^{2*}

The ability of morphine to alleviate pain is mediated through a heterotrimeric guanine nucleotide binding protein (G protein)-coupled heptahelical receptor (GPCR), the μ opioid receptor (μ OR). The efficiency of GPCR signaling is tightly regulated and ultimately limited by the coordinated phosphorylation of the receptors by specific GPCR kinases and the subsequent interaction of the phosphorylated receptors with β -arrestin 1 and β -arrestin 2. Functional deletion of the β -arrestin 2 gene in mice resulted in remarkable potentiation and prolongation of the analgesic effect of morphine, suggesting that μ OR desensitization was impaired. These results provide evidence in vivo for the physiological importance of β -arrestin 2 in regulating the function of a specific GPCR, the μ OR. Moreover, they suggest that inhibition of β -arrestin 2 function might lead to enhanced analgesic effectiveness of morphine and provide potential new avenues for the study and treatment of pain, narcotic tolerance, and dependence.

GPCRs have important roles in mediating fundamental physiological processes such as vision, olfaction, cardiovascular function, and pain perception. Cellular communication through GPCRs requires the coordination of processes governing receptor activation, desensitization, and resensitization. However, the relative contribution of desensitization mechanisms to the overall homeostatic process still remains largely unexplored in vivo. GPCR kinases (GRKs) act to phosphorylate activated receptors and promote their interaction with β -arrestins. This, in turn, prevents further coupling with G proteins and disrupts normal activation of the second messenger signaling cascade. By this mechanism, GRKs and β -arrestins can act to dampen GPCR signaling, thereby leading to desensitization of the receptor (1). At least six GRKs (GRK1 to GRK6)

and four arrestins (visual and cone arrestin, β -arrestins 1 and 2) have been discovered; however, the functional importance of such redundancy is unclear. Overexpression (2) or inactivation (3) of certain GRKs leads to modulation of receptor responsiveness. In addition, mice that are deficient in β -arrestin 1 display increased cardiac contractility in response to β adrenergic receptor agonists (4). Therefore, the use of animal models in which the genes for GRKs and β -arrestins are functionally inactivated should help to elucidate the contribution of the desensitization mechanisms to the physiological responses.

Because GPCRs, such as the substance P receptor and the opioid receptors, participate in processing the sensation of pain, we characterized analgesic responses through the μ opioid receptor (μ OR) in mice lacking β -arrestin 2. In the clinical setting, morphine is currently the most effective drug for alleviating intense and chronic pain. The antinociceptive (blocking of pain perception) actions of morphine are mediated through stimulation of the μ OR, as demonstrated by the lack of morphine analgesia observed in knockout mice deficient in the μ OR (5, 6). Nevertheless, the neuronal signaling mechanisms mediating analgesia through μ ORs and mor-

phine remain poorly understood. Moreover, the contribution of GPCR desensitization to the onset and duration of analgesia has been unclear.

We generated β -arrestin 2 knockout (β arr2-KO) mice by inactivation of the gene by homologous recombination (7). Mice lacking β -arrestin 2 were identified by Southern (DNA) blot analysis (Fig. 1A), and the absence of β -arrestin 2 was confirmed by protein immunoblotting of extracts from brainstem, periaqueductal gray (PAG) tissue, spleen, lung, and skin (Fig. 1B) (8). Because wild-type, heterozygous (β arr2^{+/-}), and homozygous mutant mice had similar amounts of β -arrestin 1 in the brain regions examined (Fig. 1B), compensatory up-regulation of β -arrestin 1 in the absence of β -arrestin 2 seems unlikely. The β arr2-KO mice were viable and had no gross phenotypic abnormalities. However, after administration of morphine, obvious differences became apparent between the genotypes.

Morphine-induced antinociception was evaluated by measuring response latencies in the hot-plate test. We used a dose of morphine (10 mg/kg body weight) and route of administration (subcutaneous) that are known to induce analgesia in many strains of mice (9). The analgesic effect of morphine was significantly potentiated and prolonged in the knockout mice relative to their wild-type littermates (Fig. 2). Such robust responses to morphine were absent not only in the wild-type littermates (Fig. 2) but also in the parental mouse strains (C57BL/6 and 129SvJ) used to generate this knockout (10). Four hours after the morphine injection, β arr2-KO mice still exhibited significant analgesia [percent maximum possible effect (MPE) = $31 \pm 0.4\%$], whereas in their wild-type littermates, the analgesic effects of the same dose of morphine waned after about 90 min. β arr2^{+/-} mice were nearly as responsive to morphine as the β arr2-KO mice; however, this may reflect the imposed limit of the hot-plate assay (30 s), which is designed to prevent prolonged exposure of the mice to pain. Basal responses to the hot plate did not differ between genotypes (wild type, 6.2 ± 0.3 s, $n = 25$; β arr2-KO, 6.1 ± 0.4 s, $n = 27$). The differences in morphine-induced analgesia between the genotypes are unlikely to

¹Howard Hughes Medical Institute Laboratories, Departments of Cell Biology and Medicine, ²Howard Hughes Medical Institute Laboratories, Departments of Biochemistry and Medicine, Duke University Medical Center, Durham, NC 27710, USA.

*These authors contributed equally to this report.

†To whom correspondence should be addressed. E-mail: lefko001@receptor-biol.duke.edu; or caron002@mc.duke.edu

‡To whom requests for materials should be addressed.

LINKED CITATIONS

- Page 1 of 1 -



You have printed the following article:

Gas-Rich Galaxy Pair Unveiled in the Lensed Quasar 0957+561

P. Planesas; J. Martin-Pintado; R. Neri; L. Colina

Science, New Series, Vol. 286, No. 5449. (Dec. 24, 1999), pp. 2493-2495.

Stable URL:

<http://links.jstor.org/sici?sici=0036-8075%2819991224%293%3A286%3A5449%3C2493%3AGGPUT%3E2.0.CO%3B2-Z>

This article references the following linked citations:

References and Notes

¹²**The Double Quasar 0957+561: Examination of the Gravitational Lens Hypothesis Using the Very Large Array**

P. E. Greenfield; D. H. Roberts; B. F. Burke

Science, New Series, Vol. 208, No. 4443. (May 2, 1980), pp. 495-497.

Stable URL:

<http://links.jstor.org/sici?sici=0036-8075%2819800502%293%3A208%3A4443%3C495%3ATDQ0EO%3E2.0.CO%3B2-L>

NOTE: *The reference numbering from the original has been maintained in this citation list.*